A finite element approach to incompressible two-phase flow on manifolds

I. Nitschke, A. Voigt and J. Wensch

Journal of Fluid Mechanics / Volume 708 / October 2012, pp 418 - 438
DOI: 10.1017/jfm.2012.317, Published online:

Link to this article: http://journals.cambridge.org/abstract_S0022112012003175

How to cite this article:
I. Nitschke, A. Voigt and J. Wensch (2012). A finite element approach to incompressible two-phase flow on manifolds. Journal of Fluid Mechanics, 708, pp 418-438 doi:10.1017/jfm.2012.317

J. Fluid Mech. (2012), *vol.* 708, *pp.* 418–438.
doi:10.1017/jfm.2012.317

A finite element approach to incompressible two-phase flow on manifolds

I. Nitschke[1], **A. Voigt**[1,2]† **and J. Wensch**[1]

[1] Institut für Wissenschaftliches Rechnen, Technische Universität Dresden, 01062 Dresden, Germany
[2] Center for Advanced Modeling and Simulation, Technische Universität Dresden, 01062 Dresden, Germany

(Received 29 September 2011; revised 17 May 2012; accepted 20 June 2012; first published online 8 August 2012)

A two-phase Newtonian surface fluid is modelled as a surface Cahn–Hilliard–Navier–Stokes equation using a stream function formulation. This allows one to circumvent the subtleties in describing vectorial second-order partial differential equations on curved surfaces and allows for an efficient numerical treatment using parametric finite elements. The approach is validated for various test cases, including a vortex-trapping surface demonstrating the strong interplay of the surface morphology and the flow. Finally the approach is applied to a Rayleigh–Taylor instability and coarsening scenarios on various surfaces.

Key words: Membranes, Multiphase flow, Navier–Stokes equations

1. Introduction

Newtonian surface fluids have been considered in various applications. The work dates back to Scriven (1960) who was interested in the importance of interface rheology on foam stability and derived a general formulation of the dynamics of a Newtonian surface fluid, which forms the interfacial boundary conditions for a two-phase flow problem of the embedding solvent. The equations of motion are formulated intrinsically in a two-dimensional manifold with time-varying metric and make extensive use of the covariant derivative, and calculations in local coordinates, which involve the coefficients of the Riemannian connection and its derivatives. The complexity of the equations may explain why they are often written but never solved for arbitrary surfaces. With a growing interest in complex fluids for which surface properties dominate due to a large area-to-volume ratio of small droplets, e.g. in emulsions or liquid phases in cell membranes, there is now also a need for an efficient numerical treatment of the equations. Within the context of cell membranes the model has been considered, for example, in Hu, Zhang & E (2007), Arroyo & DeSimone (2009) and Fan, Han & Haataja (2010). However, the numerical treatment is restricted to simplified geometries, e.g. an axisymmetric setting (Arroyo & DeSimone 2009) or a planar interface (Fan *et al.* 2010). Such special cases circumvent the subtleties in describing vectorial second-order partial differential equations on curved domains. Unlike for scalar conservation laws, a simple translation of the operators to manifold operators leads to governing equations different from those that result from the basic

† Email address for correspondence: axel.voigt@tu-dresden.de

conservation laws of physics applied to manifolds, as was done by Scriven (1960). For this reason, efficient computational tools that have been developed to solve scalar partial differential equations on manifolds, such as parametric finite elements (Dziuk & Elliott 2007*a*,*b*; Vey & Voigt 2007), level set methods (Bertalmio *et al.* 2001; Stöcker & Voigt 2008), phase-field approaches (Rätz & Voigt 2006, 2007; Elliott & Stinner 2009) or closest point methods (Ruuth & Merriman 2008; MacDonald & Ruuth 2009), cannot directly be applied to the vector case.

We will consider a special case of a two-phase flow problem with surface tension, surface viscosity and surface phase transition in which the surface decouples from the bulk. The resulting model is an incompressible two-phase flow problem on a manifold, which will be considered using a modified Navier–Stokes–Cahn–Hilliard equation on a manifold. In order to be able to solve this equation numerically, we use a stream function formulation, which results in a scalar surface partial differential equation of fourth order. A parametric finite element approach is used to solve this equation as a system of second-order equations. Various test cases are considered first without the coupling of the incompressible Navier–Stokes equation with the Cahn–Hilliard model. The full model is applied to simulate a Rayleigh–Taylor instability on a torus as well as coarsening dynamics following a spinodal decomposition process on various geometries. An outline will be given as to how to extend this approach to the full model coupled with the bulk flow of the embedding solvent.

2. Mathematical model

We follow the approach in Bothe & Pruess (2010) to introduce the mathematical model. We therefore consider two immiscible Newtonian fluids with constant densities. The fluid velocities are continuous at the phase boundary and the interface is advected with the flow. For the surface stress the Boussinesq–Scriven law is used, which is extended to incorporate different phases on the surface using a Cahn–Hilliard model. Without surface viscosity, the idea has already been used before to study phase separation dynamics in two-component vesicles (see e.g. Taniguchi 1996; Wang & Du 2008; Lowengrub, Rätz & Voigt 2009). A formal asymptotic analysis has recently been done by Elliott & Stinner (2011). The full model of a two-phase flow problem with surface tension, surface viscosity and surface phase transition thus reads:

$$\nabla \cdot \boldsymbol{u} = 0, \quad t > 0,\ x \in \Omega^i(t), \tag{2.1}$$

$$\partial_t(\rho^i \boldsymbol{u}) + \nabla \cdot (\rho^i \boldsymbol{u} \otimes \boldsymbol{u} - S) = 0, \quad t > 0,\ x \in \Omega^i(t), \tag{2.2}$$

$$S = -\pi I + 2\mu^i D, \quad t > 0,\ x \in \Omega^i(t), \tag{2.3}$$

$$D = \tfrac{1}{2}(\nabla \boldsymbol{u} + \nabla \boldsymbol{u}^{\mathrm{T}}), \quad t > 0,\ x \in \Omega^i(t), \tag{2.4}$$

with $\Omega^i(t)$ the bulk fluid domain, and ρ_i, u, π and μ_i the bulk fluid density, bulk velocity field, bulk pressure and bulk viscosity, respectively. At the interface we specify

$$[[\boldsymbol{u}]] = 0, \quad V = \boldsymbol{u} \cdot \nu = \boldsymbol{u}_\Gamma \cdot \nu, \quad t > 0\, x \in \Gamma(t), \tag{2.5}$$

$$\frac{\mathrm{D}}{\mathrm{D}t}\rho_\Gamma + \rho_\Gamma \nabla_\Gamma \cdot \boldsymbol{u}_\Gamma = 0, \quad t > 0,\ x \in \Gamma(t), \tag{2.6}$$

$$\frac{\mathrm{D}}{\mathrm{D}t}(\rho_\Gamma \boldsymbol{u}_\Gamma) = \nabla_\Gamma \cdot S_\Gamma + [[S]]\nu - \sigma_\gamma \epsilon \nabla_\Gamma \cdot (\rho_\Gamma \nabla_\Gamma c \otimes \nabla_\Gamma c), \quad t > 0,\ x \in \Gamma(t), \tag{2.7}$$

$$S_\Gamma = (\sigma_\Gamma + (\lambda_\Gamma - \mu_\Gamma)\nabla_\Gamma \cdot \boldsymbol{u}_\Gamma)P_\Gamma + 2\mu_\Gamma D_\Gamma, \quad t > 0,\ x \in \Gamma(t), \tag{2.8}$$

$$D_\Gamma = \tfrac{1}{2}P_\Gamma(\nabla_\Gamma \boldsymbol{u}_\Gamma + \nabla_\Gamma \boldsymbol{u}_\Gamma^{\mathrm{T}})P_\Gamma, \quad t > 0,\ x \in \Gamma(t), \tag{2.9}$$

$$\frac{\mathrm{D}}{\mathrm{D}t}(\rho_\Gamma c) + \rho_\Gamma \boldsymbol{u}_\Gamma \cdot \nabla_\Gamma c = \sigma_\gamma \nabla_\Gamma \cdot (M(c)\nabla_\Gamma \omega), \quad t > 0,\ x \in \Gamma(t), \tag{2.10}$$

$$\omega = \frac{1}{\epsilon} G'(c) - \frac{\epsilon}{\rho_\Gamma} \nabla_\Gamma \cdot (\rho_\Gamma \nabla_\Gamma c), \quad t > 0,\ x \in \Gamma(t), \tag{2.11}$$

with $\Gamma(t)$ the bulk fluid–fluid interface, ρ_Γ the interfacial density, $\boldsymbol{u}_\Gamma$ the interfacial velocity, λ_Γ the dilatational viscosity, μ_Γ the surface viscosity, σ_Γ the surface tension and σ_γ the line tension. The two-phase surface fluid is modelled using a surface phase-field model, which is an extension of Lowengrub & Truskinowsky (1998) with an order parameter c, distinguishing the two surface fluid phases, a chemical potential ω, a double-well potential $G(c) = c^2\,(1-c)^2\,/4$, a mobility function $M(c) = \sqrt{c^2\,(1-c)^2}$ and a small parameter ϵ specifying the length scale on which the surface fluid–fluid interface $\gamma(t)$ is smeared out. Furthermore, we have ν the unit outer normal at $\Gamma(t)$, $P_\Gamma = \boldsymbol{I} - \nu \otimes \nu$ the tangential projection at $\Gamma(t)$, with $\boldsymbol{I}$ the identity matrix, and $\mathrm{D}/\mathrm{D}t = \partial_t + (\boldsymbol{u} \cdot \nabla)$ the Lagrangian derivative. The tangential gradient on $\Gamma(t)$ for any function η defined in an open subset containing $\Gamma(t)$ is defined as $\nabla_\Gamma \eta = \nabla \eta - \nabla \eta \cdot \nu \nu$ with the usual scalar product and the usual gradient. The tangential gradient thereby only depends on the values restricted to $\Gamma(t)$ and $\nabla_\Gamma \eta \cdot \nu = 0$. The components of the tangential gradient are denoted by $\nabla_\Gamma \eta = (D_1 \eta, \ldots, D_{n+1}\eta)$ and the Laplace–Beltrami operator on $\Gamma(t)$ is defined as $\Delta_\Gamma = \nabla_\Gamma \cdot \nabla_\Gamma \eta = \sum_{i=1}^{n+1} D_i D_j \eta$. In addition we specify $\boldsymbol{u}(0,x) = \boldsymbol{u}_0(x)$ for $x \in \Omega^i(0)$, $c(0,x) = c_0(x)$ for $x \in \Gamma(0) = \Gamma_0$ and $\boldsymbol{u} = 0$ for $x \in \partial\Omega$, with $\Omega = \Omega^1(t) \cup \Gamma(t) \cup \Omega^2(t)$ a fixed domain, for which we assume $\Gamma(t) \cap \partial\Omega = \emptyset$.

We introduce the hydrodynamic length $l_{hy} = \mu_\Gamma/\mu_i$, which distinguishes two-dimensional from three-dimensional flow for spatial scales smaller than or greater than l_{hy} (Safmann & Delbrueck 1975). We will consider the regime of $l_{hy} \to \infty$ for which the surface flow decouples from the bulk. This regime is an idealized approximation of a typical situation in fluid vesicles, with a more viscous surface fluid (lipids) surrounded by liquid (water). We split the interfacial velocity into a tangential and a normal component $\boldsymbol{u}_\Gamma = \boldsymbol{v} + V\nu$ and assume $V = 0$. This requires a stationary shape, which, for example, follows for spherical fluid vesicles and is a mathematical consequence of a constant volume and surface area; see Veatch & Keller (2003) and Yanagisawa *et al.* (2007) for experimental results on domain growth on stationary shapes. We further assume ρ_Γ is a constant and set $\rho_\Gamma = 1$, which now is possible as changes of mass density on the surface, e.g. due to stretching of the surface, are no longer possible. We thus obtain $\nabla_\Gamma \cdot \boldsymbol{u}_\Gamma = 0$. All interfacial quantities are assumed to be constantly extended in the normal direction off the interface. With these assumptions, the convective surface Cahn–Hilliard model reduces to

$$\partial_t c + \boldsymbol{v} \cdot \nabla_\Gamma c = \sigma_\gamma \nabla_\Gamma \cdot (M(c)\nabla_\Gamma \omega), \tag{2.12}$$

$$\omega = \frac{1}{\epsilon} G'(c) - \epsilon \Delta_\Gamma c. \tag{2.13}$$

The surface flow problem for $\boldsymbol{v}$ on a manifold reads

$$\partial_t \boldsymbol{v} + \boldsymbol{v} \cdot \nabla_\Gamma \boldsymbol{v} = -\nabla_\Gamma \tilde{p} + 2\mu_\Gamma \nabla_\Gamma \cdot D_\Gamma + \tilde{F}, \tag{2.14}$$

$$\nabla_\Gamma \cdot \boldsymbol{v} = 0, \tag{2.15}$$

where $\tilde{p} = -\sigma_\Gamma$ denotes the thermodynamic interfacial pressure (here the surface tension (see Scriven 1960)), $\tilde{F} = -\sigma_\gamma \epsilon \nabla_\Gamma \cdot (\nabla_\Gamma c \otimes \nabla_\Gamma c)$ a forcing term, accounting for line tension effects, and H denotes the total mean curvature of $\Gamma(t)$. Following Feng (2006) this can be reformulated using $p = \tilde{p} + (\sigma_\gamma \epsilon/2)\,|\nabla_\Gamma c|^2 + (\sigma_\gamma/2) G(c)$

and $F = -\sigma_\gamma \epsilon \omega \nabla_\Gamma c$ into

$$\partial_t \boldsymbol{v} + \boldsymbol{v} \cdot \nabla_\Gamma \boldsymbol{v} = -\nabla_\Gamma p + 2\mu_\Gamma \nabla_\Gamma \cdot D_\Gamma + F, \tag{2.16}$$

$$\nabla_\Gamma \cdot \boldsymbol{v} = 0. \tag{2.17}$$

In the following we will also allow for other forces F in this setting.

Before we proceed, consider the special case of a flat surface. We obtain

$$\partial_t c + \boldsymbol{v} \cdot \nabla c = \sigma_\gamma \nabla \cdot (M(c) \nabla \omega), \tag{2.18}$$

$$\omega = \frac{1}{\epsilon} G'(c) - \epsilon \Delta c, \tag{2.19}$$

$$\partial_t \boldsymbol{v} + \boldsymbol{v} \cdot \nabla \boldsymbol{v} = -\nabla p + 2\mu_\Gamma \nabla \cdot D + F, \tag{2.20}$$

$$\nabla \cdot \boldsymbol{v} = 0, \tag{2.21}$$

with $D = (\nabla \boldsymbol{v} + \nabla \boldsymbol{v}^{\mathrm{T}})/2$ and $F = -\sigma_\gamma \epsilon \omega \nabla c$. The resulting model is the classical 'model H' (see Hohenberg & Halperin 1977). The zero-divergence condition enables one to set $\boldsymbol{v} = \nabla \times \psi$ with a stream function ψ. Applying the operator $\mathrm{rot} = \nabla \times$ to the Navier–Stokes equation now cancels the gradient terms and the nonlinear advection operator transforms to $\boldsymbol{v} \cdot \nabla \boldsymbol{v} = J(\psi, \Delta\psi)$, where $J(a, b) = a_x b_y - a_y b_x$ is the so-called Jacobian. Furthermore the viscous term results in a biharmonic $\Delta\Delta\psi$ and we obtain

$$\partial_t c + J(\psi, c) = \sigma_\gamma \nabla \cdot (M(c) \nabla \omega), \tag{2.22}$$

$$\omega = \frac{1}{\epsilon} G'(c) - \epsilon \Delta c, \tag{2.23}$$

$$\partial_t \Delta\psi + J(\psi, \Delta\psi) = \mu_\Gamma \Delta^2 \psi + f, \tag{2.24}$$

with $f = \mathrm{rot}\, F$.

This procedure can be generalized to a two-dimensional Riemannian manifold. The necessary generalizations are given in the Appendix. We point out that these can be given in intrinsic terms without specifying an embedding of the manifold into $\mathbb{R}^3$. Following Arroyo & DeSimone (2009) the term $\nabla_\Gamma \cdot D_\Gamma$ can be expressed through a geometric form in the spirit of Scriven (1960). Using a generalized Laplacian of a vector field on a manifold, we obtain from such a setting

$$\partial_t \boldsymbol{v} + \boldsymbol{v} \cdot \nabla_\Gamma \boldsymbol{v} = -\nabla_\Gamma p + \mu_\Gamma (\Delta_\Gamma^B \boldsymbol{v} + K\boldsymbol{v}) + F, \tag{2.25}$$

with Δ_Γ^B the so-called Bochner or rough Laplacian, and K the Gaussian curvature. This formulation but without the Gaussian curvature term has been used in Temam (1988) to formulate the Navier–Stokes equation on a manifold. An alternative formulation is

$$\partial_t \boldsymbol{v} + \boldsymbol{v} \cdot \nabla_\Gamma \boldsymbol{v} = -\nabla_\Gamma p + \mu_\Gamma (\Delta_\Gamma^R \boldsymbol{v} + 2K\boldsymbol{v}) + F, \tag{2.26}$$

with Δ_Γ^R the so-called Laplace–de Rham operator or Hodge–de Rham Laplacian. This formulation is used in Cao, Rammaha & Titi (1999), but again without the Gaussian curvature term. The correct formulation has been considered in the mathematical literature before in Ebin & Marsden (1970) and Mitrea & Taylor (2001). Introducing the stream function ψ we end up with a scalar partial differential equation on a manifold

$$\partial_t \Delta_\Gamma \psi + J(\psi, \Delta_\Gamma \psi) = \mu_\Gamma (\Delta_\Gamma^2 \psi + 2\nabla_\Gamma \cdot (K \nabla_\Gamma \psi)) + f, \tag{2.27}$$

where J is the Jacobian, and $f = \mathrm{rot}\, F$, with the operators J and rot defined in the Appendix. A detailed derivation of this equation is outlined in the Appendix.

The convective surface Cahn–Hilliard equation then reads

$$\partial_t c + J(\psi, c) = \sigma_\gamma \nabla_\Gamma \cdot (M(c) \nabla_\Gamma \omega), \tag{2.28}$$

$$\omega = \frac{1}{\epsilon} G'(c) - \epsilon \Delta_\Gamma c. \tag{2.29}$$

The resulting model only involves scalar quantities and can be solved with any of the numerical approaches to solve partial differential equations on manifolds mentioned in the introduction.

3. Numerical approach

Within the numerical approach we rewrite (2.27) as a system of two second-order equations and consider

$$\partial_t \phi + J(\psi, \phi) = \mu_\Gamma (\Delta_\Gamma \phi + 2 \nabla_\Gamma \cdot (K \nabla_\Gamma \psi)) + f, \tag{3.1}$$

$$\phi = \Delta_\Gamma \psi, \tag{3.2}$$

with appropriate initial conditions $\psi(x, 0) = \mathrm{rot}^{-1} u_0$. Neglecting the convective terms, the stream function approach converts the saddle point problem to a system of elliptic problems, thus no inf–sup condition has to be checked for the choice of finite elements. We will here consider a parametric finite element approach to solve the problem, following the general approach described in Dziuk & Elliott (2007*a*,*b*) and Vey & Voigt (2007).

Let Γ_h be a surface triangulation of Γ of mesh size h and let T_τ be a partition of the time interval of mesh size τ. We define the discrete time derivative $d_t v^m := (v^m - v^{m-1})/\tau$ and introduce the surface finite element spaces

$$V_h = \{v_h \in H^1(\Gamma_h) \mid v_{h|T} \in P^1 \ \forall \ T \in \Gamma_h\}. \tag{3.3}$$

The surface finite element approximation for the vorticity equations (3.1) and (3.2) thus reads as follows. Find $(\phi^m, \psi^m) \in V_h \times V_h$ such that for all $(\alpha, \beta) \in V_h \times V_h$

$$(d_t \phi^m, \alpha) + (J(\psi^{m-1}, \phi^m), \alpha) = \mu_\Gamma (\nabla_\Gamma \phi^m, \nabla_\Gamma \alpha) - 2\mu_\Gamma (K \nabla_\Gamma \psi^m, \nabla_\Gamma \alpha) + (f, \alpha), \tag{3.4}$$

$$(\phi^m, \beta) = -(\nabla_\Gamma \psi^m, \nabla_\Gamma \beta). \tag{3.5}$$

The finite element approximation for the convective Cahn–Hilliard equation then reads as follows. Find $(c^m, \omega^m) \in V_h \times V_h$ such that for all $(\gamma, \delta) \in V_h \times V_h$

$$(d_t c^m, \gamma) + (J(\psi^m, c^m), \gamma) - \sigma_\gamma (M(c^{m-1}) \nabla \omega^m, \nabla \gamma) = 0, \tag{3.6}$$

$$(\omega^m, \delta) + \epsilon (\nabla c^m, \nabla \delta) - \frac{1}{\epsilon} (G'(c^m), \delta) = 0. \tag{3.7}$$

Furthermore, we linearize the derivative of the double-well potential $G'(c^m)$ by a Taylor expansion of order one, $G'(c^m) \approx (c^{m-1})^3 - c^{m-1} + (3\,(c^{m-1})^2 - 1)(c^m - c^{m-1})$, to obtain a linear system but keeping the nonlinearity (semi-)implicit. The forcing term in the vorticity equation is treated explicitly and reads $(f, \alpha) = \sigma_\gamma (J(\omega^{m-1}, c^{m-1}), \alpha)$. In each time step we thus first solve the vorticity equation, obtaining ψ^m, and afterwards solve the convective Cahn–Hilliard equation to obtain c^m and ω^m. The discretization in space and time is consistent with the corresponding approach for flat surfaces (see e.g. Aland & Voigt 2012). The time step is thereby restricted by dynamical events in the Cahn–Hilliard equation and is chosen adaptively based on an accuracy criteria. This behaviour is consistent with the findings of an unconditionally stable scheme for the Cahn–Hilliard equation (Gomez & Hughes 2011). If not given analytically, which

is only possible for specific surfaces, the numerical approach requires one also to approximate the total mean and the Gaussian curvature H and K using the information of the surface triangulation Γ_h. The curvatures are given in terms of the surface normal by

$$H = \nabla \cdot \nu, \tag{3.8}$$

$$K = \frac{1}{2}\left((\nabla \cdot \nu)^2 - \sum_{i=1}^{3}\sum_{j=1}^{3} \left(\frac{\partial \nu_j}{\partial x_i} \right)^2 \right). \tag{3.9}$$

As Γ_h is only a globally C^0 piecewise polynomial surface, the normal ν is given as a piecewise constant function. A direct application of the above equations is therefore not possible. Various attempts have been made in computer graphics to deal with this problem. They are mostly based on local weighted averaging (see e.g. Meyer *et al.* 2003). Within a first approach (I), we follow this attempt and restore the normal as a smooth function using suitable interpolation procedures that are based on recovery strategies (Zienkiewicz & Zhu 1987). We demonstrate first-order convergence for two different polygonal meshes; see table 1. However, we must point out that these results are highly sensitive to the regularity of the mesh. Furthermore the approach might fail for adaptively refined meshes (see Bonito, Nochetto & Pauletti 2010). Therefore we consider also a different approach, denoted (II), to approximate the total mean and the Gaussian curvature H and K, which is based on a finite element approximation and is commonly used in the approximation of geometric evolution equations (see e.g. Dziuk 1991). We here follow Heine (2004), in which a weak formulation for the Weingarten map $\Pi = \nabla_\Gamma \nu$ and the identity $\boldsymbol{H} = -\Delta_\Gamma \boldsymbol{X}$ is used to compute H and K. Thereby $\boldsymbol{X}$ denotes the position vector and $\boldsymbol{H}$ the vector curvature. The order of convergence with respect to the L_2-norm was shown to be $k-1$, if k is the degree of the isoparametric Lagrange elements (see Heine 2004). As $k = 1$ in our case, this would indicate no convergence. We therefore modify the approach slightly by using a gradient recovery strategy to approximate $\nabla_\Gamma \boldsymbol{X}$ as a piecewise linear function. We again demonstrate convergence for two different polygonal meshes, see table 1, which show an order of convergence of $1/2$ and 1, depending on the mesh. For more irregular meshes the approach fails to converge, which is in agreement with the numerical results in Heine (2004), in which a highly irregular mesh has been used. The mentioned problems with adaptively refined meshes still remain. As a last approach, denoted (III), we use Lagrange elements of degree $k = 2$ within the original approach of Heine (2004) and project the inner nodes of the surface triangulation to Γ. The obtained convergence results are shown in table 1. We see second-order convergence for both meshes. The results are much less sensitive to the regularity of the mesh and the approach is also suitable for adaptively refined meshes. The convergence rate drops for such cases but for all considered meshes at least first-order convergence was achieved. This again is in agreement with Heine (2004). With these findings the last method is the most suitable; however, the drawback of the approach is the need for higher-order isoparametric elements or, as in our case, a projection of inner nodes to Γ, which in general might not be known.

The accuracy of all the considered approaches depends on the quality of the surface mesh and thus limits the accuracy of the whole algorithm if applied for complicated surfaces with irregular surface meshes. However, for smooth surfaces and an appropriate surface mesh, all the approaches are sufficient, as long as adaptivity is not used. For the considered examples of a sphere and a torus, we further demonstrate this by comparing results for the flow field if an analytic form for H and K is used or

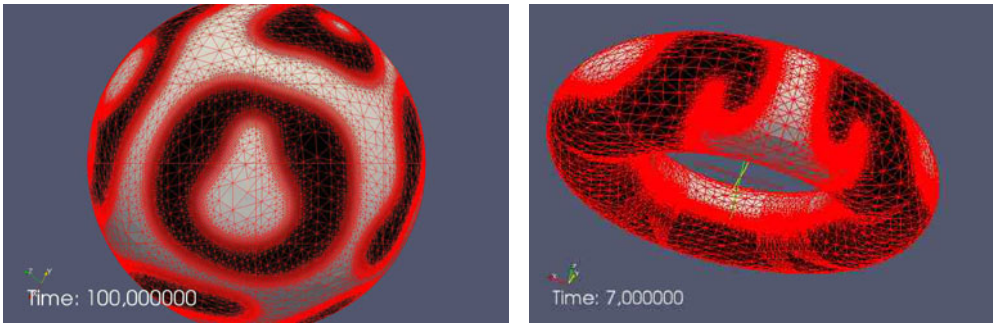

FIGURE 1. (Colour online) Adaptively refined surface mesh for a sphere and a torus. An L^2-like error indicator is used to refine the mesh along the diffuse interface with $c = 0.5$. New mesh points are projected onto Γ.

	h	$e_{L^2}(K_I)$	EOC	$e_{L^2}(K_{II})$	EOC	$e_{L^2}(K_{III})$	EOC
Icosahedral grid	1.051 460	0.825 140		0.555 163		2.228 640	
	0.618 034	0.357 732	1.57	0.527 720	0.10	0.581 252	2.53
	0.324 920	0.124 774	1.63	0.279 096	0.99	0.141 596	2.19
	0.164 647	0.060 118	1.07	0.184 701	0.61	0.034 723	2.07
	0.082 604	0.030 395	0.99	0.129 955	0.51	0.008 603	2.02
	0.041 337	0.015 944	0.93	0.092 174	0.50	0.002 142	2.01
	0.020 673	0.008 695	0.87	0.065 294	0.50	0.000 534	2.00
Cubed sphere grid	0.088 388	0.025 502		0.053 963		0.004 289	
	0.044 194	0.012 742	0.93	0.027 142	1.01	0.001 066	1.86
	0.022 097	0.006 406	0.95	0.013 671	1.02	0.000 266	2.14
	0.011 048	0.003 238	0.99	0.006 982	1.04	0.000 066	2.13

TABLE 1. Errors of the computed Gaussian curvature K in the L_2-norm for an icosahedral and a cubed sphere grid and estimated orders of convergence (EOC) for different methods: (I) local weighted averaging, (II) weak formulation with piecewise linear finite elements and piecewise linear approximation of the gradient of the position vector, and (III) weak formulation with piecewise quadratic finite elements and projection of inner nodes to the exact surface.

the numerical approximation (I); see table 3. Approach (I) is also used for the example of a perturbed sphere for which H and K are not known analytically; see results in § 4. The underlying mesh has the same structure as a cubed sphere grid, and is only locally perturbed. In all other examples we use the analytic form for H and K.

The adaptive finite element toolbox AMDiS (Vey & Voigt 2007) is used for discretization. The linearized systems are solved using the direct unsymmetric multifrontal method (UMFPACK). Adaptive meshes are indispensable for providing a high spatial resolution along the phase boundary described implicitly by c. Here we use the value of c as an indicator of where to refine or coarsen the mesh. As long as Γ is known, new grid points inserted in Γ_h will be projected on Γ to reduce the approximation error. Figure 1 shows a typical mesh on a sphere and a torus. If on the other hand the information of the geometry is only incomplete and only the surface triangulation Γ_h is known, mesh modifications have to be done in

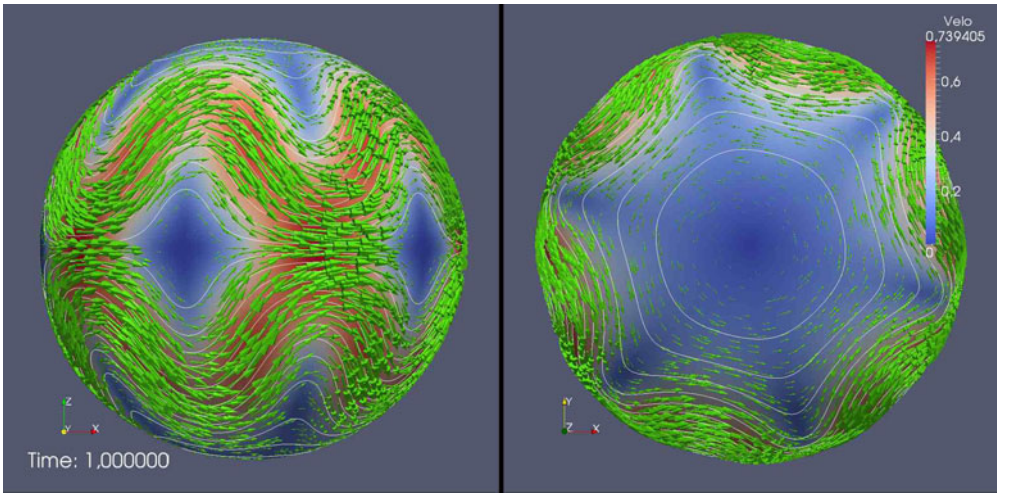

FIGURE 2. (Colour online) Numerical solution for stationary rotating sphere problem. The velocity together with the streamlines from different viewpoints are shown.

a geometrically consistent way (Bonito *et al.* 2010) to preserve accuracy on position, total mean and Gaussian curvature. In the numerical examples we only use a given surface triangulation without adaptive mesh refinement if an analytic expression for Γ is not available; see § 4.

4. Validation and test cases

To validate the numerical approach for surface flow we consider the following simplified single-phase flow problem. We first follow an approach in meteorology and consider the motion of harmonic waves in the atmosphere. We use a rotating sphere as our computational domain. The Coriolis force is incorporated into the model by considering $J(\psi, \phi + l)$ with the Coriolis parameter $l = 2\omega \sin\varphi$, angular frequency ω and latitude φ. If we further neglect the viscosity and force terms the system reduces to

$$(d_t\phi^m, \alpha) + (J(\psi^{m-1}, \phi^m), \alpha) + (J(\psi^m, l), \alpha) = 0, \tag{4.1}$$

$$(\phi^m, \beta) = -(\nabla_\Gamma \psi^m, \nabla_\Gamma \beta), \tag{4.2}$$

and has the stationary solution $\psi(\varphi, \lambda) = a \sin(l\lambda) P_n^l(\sin\varphi) - 2\omega \sin\varphi/[K(n(n+1)-2)]$, with $a \in R$, $l, n \in N$ $(l \leqslant n)$, λ the longitude and P_n^l the Legendre polynomial (see Neamtan 1946). Figure 2 shows the numerical solution for $K = 1$, $l = 6$, $n = 7$, $a = 0.000\,002\,741$ and $\omega = 10$. Table 2 demonstrates second-order convergence of the numerical approach in the maximum norm.

Inspired by this stationary example we construct a time-dependent analytical solution for the original problem with viscosity and force terms. The solution reads $\psi(\varphi, \lambda, t) = \sin\varphi \cos^6\varphi \, \varphi \sin(6\lambda) g(t)$, which is obtained by using $K = 1$, $m = 6$, $n = 7$, $a = 0.000\,007\,400$ and $\omega = 0$. We use $g(t) = -2t + 1$. As $J(\psi, \phi) = 0$ we obtain $f = -56 \sin\varphi \cos^6\varphi \, \sin(6\lambda)(-2 + 54\mu_\Gamma g(t))$. The system to be solved reads

$$(d_t\phi^m, \alpha) = \mu_\Gamma(\nabla_\Gamma \phi^m, \nabla_\Gamma \alpha) - 2\mu_\Gamma(K\nabla_\Gamma \psi^m, \nabla_\Gamma \alpha) + (f, \alpha), \tag{4.3}$$

$$(\phi^m, \beta) = -(\nabla_\Gamma \psi^m, \nabla_\Gamma \beta). \tag{4.4}$$

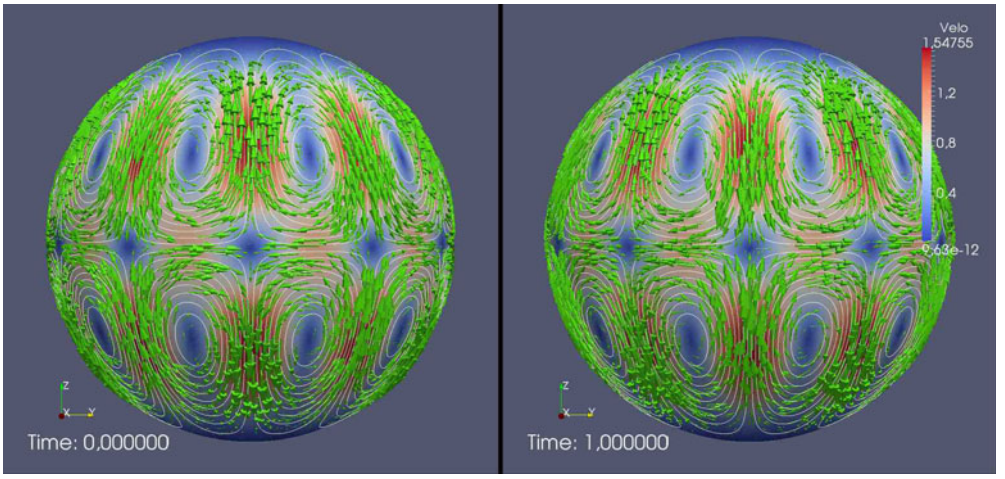

FIGURE 3. (Colour online) Numerical solution for time-dependent non-rotating sphere. The velocity together with the streamlines at different times are shown.

N	e_{L^∞}	EOC
770	0.027 4569	
1 538	0.015 6816	0.81
3 074	0.007 9293	0.98
6 146	0.004 4774	0.82
12 290	0.002 1566	1.05
24 578	0.001 1472	0.91
49 154	0.000 5500	1.06
98 306	0.000 2889	0.93

TABLE 2. Stationary rotating sphere problem: L^∞-error and experimental order of convergence (EOC).

Figure 3 shows the numerical solution for $\mu_\Gamma = 0.1$ at $t = 0$ and after 100 time steps at $t = 1$. Table 3 demonstrates again second-order convergence of the numerical approach in the maximum norm. We have computed the convergence rate with $K = 1$ given, as well as K computed from the surface mesh using approach (I), which does not have an effect on the convergence rate in this particular example.

In order to demonstrate the applicability of the approach we consider a rotating sphere with a source term $f(x, y, z) = 20y$ for $\sqrt{y^2 + z^2} < 0.2$ and $x > 0$ and $f = 0$ otherwise. The system to be solved reads

$$\begin{aligned}(d_t\phi^m, \alpha) + (J(\psi^{m-1}, \phi^m), \alpha) - (J(\psi^m, l), \alpha)\\ = \mu_\Gamma(\nabla_\Gamma\phi^m, \nabla_\Gamma\alpha) - 2\mu_\Gamma(K\phi^m, \alpha) + (f, \alpha),\end{aligned} \tag{4.5}$$

$$(\phi^m, \beta) = -(\nabla_\Gamma\psi^m, \nabla_\Gamma\beta). \tag{4.6}$$

Here we have used $(\nabla_\Gamma\psi^m \cdot \nabla_\Gamma K, \alpha) = 0$ if $K = 1$. Figure 4 shows the numerical solution for $\mu_\Gamma = 0.05$ after 10 time steps at $t = 0.1$ for different values of ω .

As a last example we use a similar setting, but without the Coriolis force, on a more complicated surface to validate the influence of the surface morphology on the

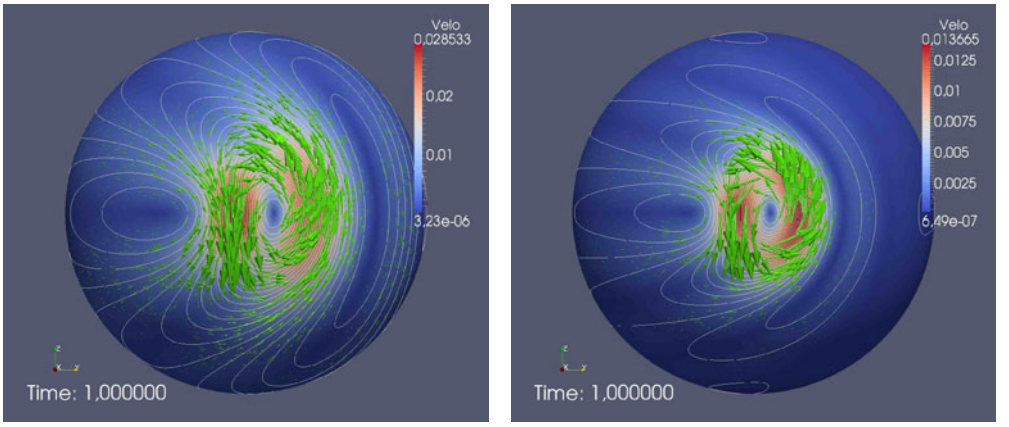

FIGURE 4. (Colour online) Numerical solution for time-dependent rotating sphere problem. The velocity together with the streamlines for $\omega = 10$ and 50 at $t = 1$ are shown.

N	e_{L^∞}	EOC	$e_{L^\infty,K}$	EOC_K
770	0.027 5380		0.027 4821	
1 538	0.018 4179	0.58	0.018 3892	0.58
3 074	0.008 4335	1.13	0.008 4361	1.13
6 146	0.004 7253	0.84	0.004 7170	0.84
12 290	0.002 3489	1.01	0.002 3502	1.01
24 578	0.001 2034	0.96	0.001 2014	0.97
49 154	0.000 6380	0.92	0.000 6285	0.91
98 306	0.000 3016	1.08	0.000 3012	1.08

TABLE 3. Time-dependent non-rotating sphere problem: L^∞-error and experimental order of convergence (EOC), if K is given and numerically computed using the geometric information of the surface mesh (indicated by $_K$).

flow field. In this example the surface Γ is not given analytically and all geometric quantities have to be computed from the surface triangulation Γ_h. We again use approach (I). A benchmark problem with an analytical solution cannot be expected, but various theoretical ideas and experimental investigations have been devoted to the delicate interplay between surface geometry and condensed matter order on the surface; see e.g. the review articles by Bowick & Giomi (2009) and Turner, Vitelli & Nelson (2010). This coupling plays a role in determining the shape of biological structures, such as viral shells and cell membranes, and introduces defects, such as disclinations and grain boundary scars, in liquid crystals and crystalline layers. More surprising is the existence of a coupling between defects in a surface fluid and the curvature of the surface, which follow from the same geometric arguments. This has been theoretically investigated for vortices in a superfluid thin layer by Turner *et al.* (2010). To trap a vortex a non-symmetric surface is investigated. A flat surface is perturbed by an exponentially decaying variation of the form $h(x, y) = (\alpha/r_0)(x^2 - \lambda y^2)\exp(-(x^2+y^2)/2r_0^2)$ in order to create a locally saddle-shaped region. Using a Green's function for a flat surface the vertex–curvature interaction energy can be computed, showing that a vertex is indeed confined at the centre of

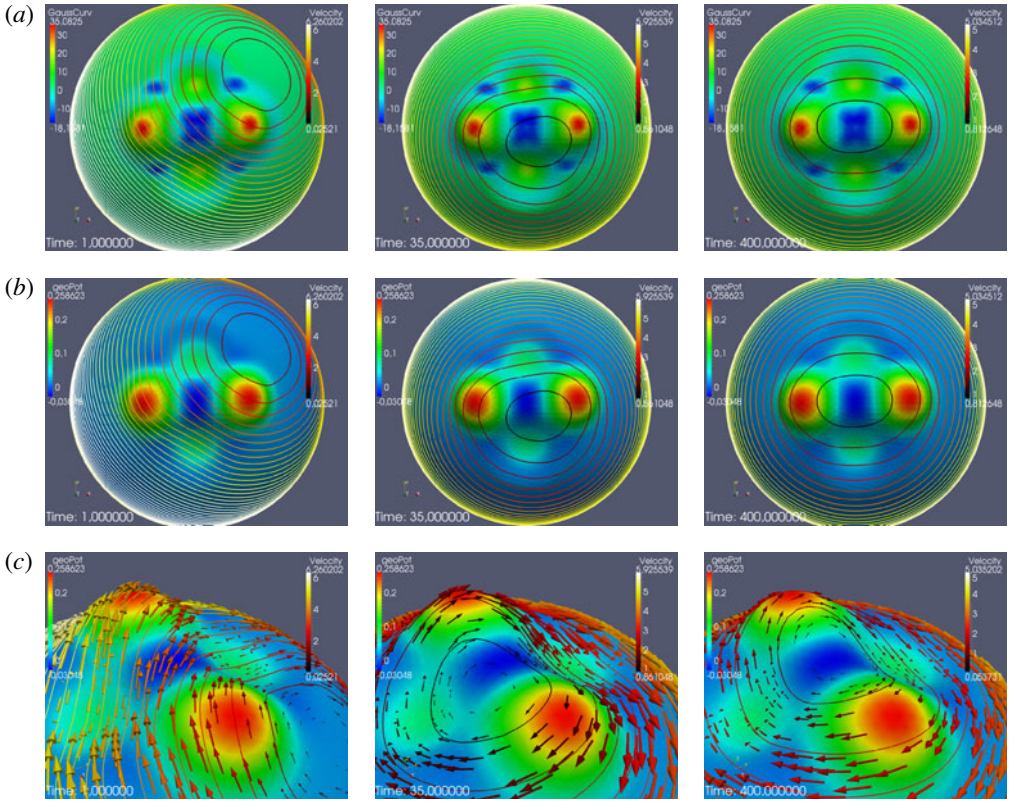

FIGURE 5. (Colour online) Time evolution of a vortex on a Gaussian saddle placed on a sphere: (*a*) full view, showing the computed Gaussian curvature K; (*b*) full view, showing the geometric potential; and (*c*) zoomed-in view. A second vortex is positioned opposite on the other side. The colour scale is according to the Gaussian curvature or the vortex–curvature interaction energy of the surface, the geometric potential U_G (see Turner *et al.* 2010). The colour coding of the isolines and the vectors is according to the velocity.

the saddle. We use the same configuration but perturb a sphere and not a flat surface. We further do not consider a superfluid thin layer but a setting with surface viscosity $\mu_\Gamma = 0.05$. This rules out any analytical treatment. Figure 5 shows the computed evolution of the vortex over time and its trapping in the Gaussian saddle. In addition, the computed Gaussian curvature K and the geometric potential U_G are plotted, which are obtained by solving the surface Poisson equation with the Gaussian curvature K acting as a source $\Delta_\Gamma U_G = K$. Again the computation is done using piecewise linear finite elements and the right-hand side K computed using strategy (I). The minimum of the geometric potential and the trapping of the vortex in the centre of the saddle are clearly seen.

5. Results for two-phase surface flow

We consider two examples, starting first with a Rayleigh–Taylor instability. Therefore we place a fluid with a larger density on top of a fluid with a lower density. The density ratio is 0.9, which allows one to incorporate the effect through a Boussinesq approximation in the forcing term f. A more general treatment with

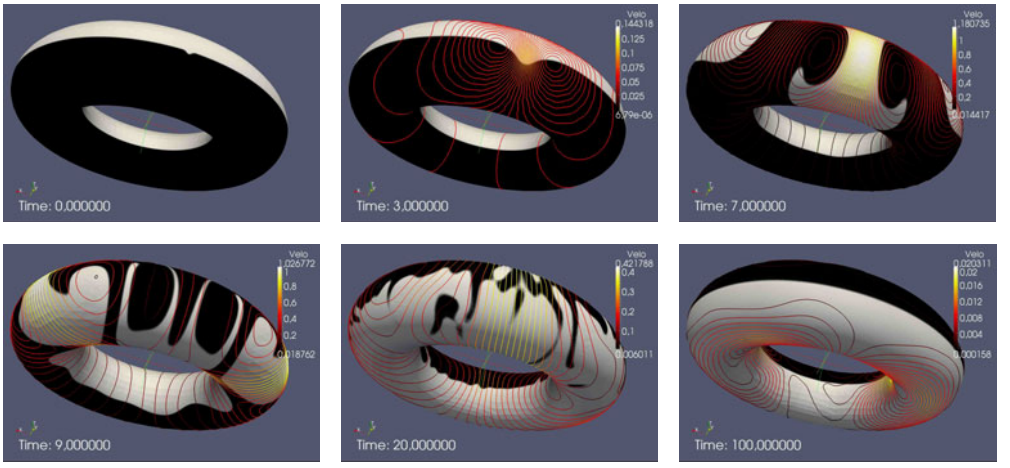

FIGURE 6. (Colour online) Time-dependent solution for Rayleigh–Taylor instability on a torus at various times. The stream function and the phase-field variable are shown.

larger density ratios could be done following the phase-field approaches for two-phase incompressible flow discussed in Aland & Voigt (2012). Figure 6 shows a sequence of the evolution on a torus. Shown is the phase-field function together with the streamlines. The parameters used are $\epsilon = 0.02$, $\sigma_\gamma = 0.001$ and $\mu_\Gamma = 0.05$.

As a second example we show the coarsening dynamics of a two-phase system following a spinodal decomposition process. We therefore compare the evolution with and without flow. Figure 7 shows a sequence of the evolution on a sphere. Shown again is the phase-field function together with the streamlines. The parameters used remain the same. The initial solution is given by $c = 0.5 \pm \eta$, with a noise term η.

Similar coexisting liquid phases on a micrometre-scale have been observed experimentally over a wide range of temperatures and lipid compositions in giant unilamellar vesicles (see e.g. Veatch & Keller 2003). The morphology of the vesicle thereby remained almost stationary, which allows at least a qualitative comparison with our results. Experiments probing these phase separation dynamics by measuring the average domain size over time lead to very different results (Saeki, Hamada & Yoshikawa 2006; Yanagisawa *et al.* 2007) and do not agree with other computational studies for these systems, which are based on dissipative particle dynamics (Laradji & Kumar 2006; Ramachandran, Laradji & Kumar 2009; Ramachandran, Komura & Gompper 2010); for a detailed comparison of the approaches, see the discussion in Fan *et al.* (2010). Here we could demonstrate that the hydrodynamic flow strongly affects the spinodal decomposition kinetics. Both simulations clearly show a faster coarsening process with fluid flow, which might help to explain the discrepancy in experimentally and computationally observed scaling results. In both examples an analytic form for K is used.

6. Conclusions

Various numerical methods have been proposed to solve partial differential equations on arbitrary surfaces. The application of these methods, however, is restricted to scalar problems. The complexity of vector-valued equations on surfaces, which make use of the covariant derivative, and calculations in local coordinates, which involve the coefficients of the Riemannian connection and its derivatives, are more

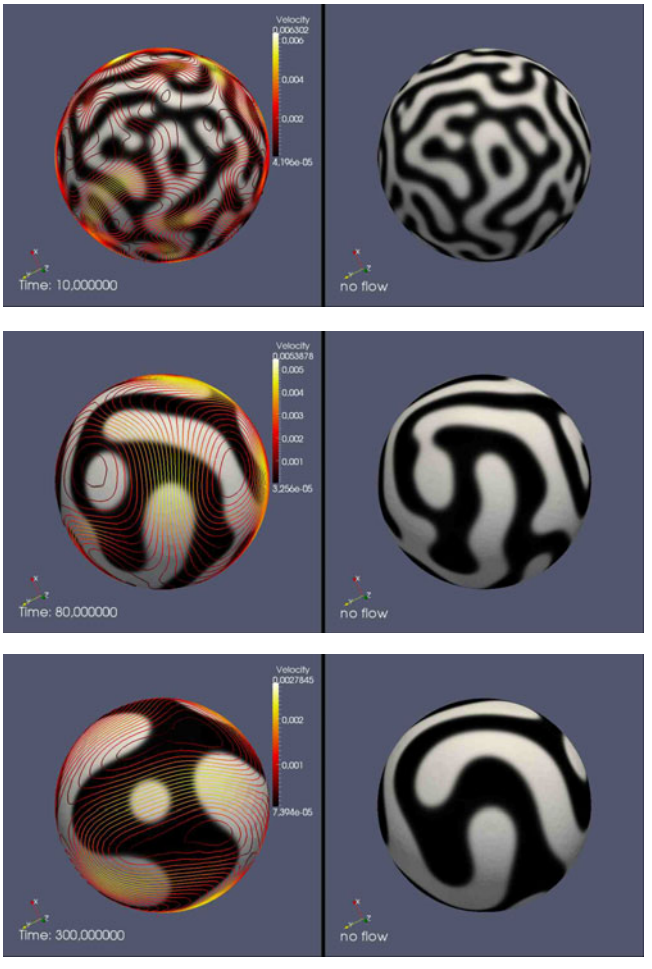

FIGURE 7. (Colour online) Time-dependent solution for coarsening on a sphere at various times, with and without flow. The stream function and the phase-field variable are shown.

complicated. This might explain why models for surface fluids are often written but never solved for arbitrary surfaces. Here we overcome this difficulty by using a stream function formulation. This results in a scalar surface partial differential equation of fourth order. A parametric finite element approach is used to solve this equation as a system of two second-order equations. Various test cases are considered, which demonstrate the applicability of the approach for an incompressible surface Navier–Stokes equation. One computational example is used to show the interplay of surface morphology and flow patterns, which has to be further investigated. Furthermore the model is extended to consider two-phase flow problems on a manifold using a surface Navier–Stokes–Cahn–Hilliard model. The full model is applied to simulate a Rayleigh–Taylor instability as well as coarsening dynamics following a spinodal decomposition process on various geometries. The last example is related to coarsening dynamics in multicomponent biomembranes.

So far the surface model is restricted to stationary surfaces. An extension to evolving surfaces is possible as long as the incompressibility constraint $\nabla_\Gamma \cdot \boldsymbol{v} = 0$

remains. The used numerical approach requires a computation of the mean curvature H and the Gaussian curvature K. If not known analytically, these have to be obtained from the surface mesh. We considered three different approaches. The accuracy of these approaches strongly depends on the quality of the surface mesh and thus limits the applicability for complicated surfaces and any extension towards the full model introduced in § 2. As an alternative computational approach we thus suggest the use of a diffuse interface approximation according to Rätz & Voigt (2006) and Li *et al.* (2009). The surface is then only implicity defined using a phase-field function φ from which the mean and Gaussian curvature can be computed (see Kwon, Thornton & Voorhees 2010). The dependence on the quality of the surface mesh is thereby circumvented, at the expense of a higher computational cost, as this approach requires the solution of a three-dimensional problem. Within the diffuse interface approach, an extension to evolving surfaces is straightforward and thus also an extension to the full model introduced in § 2 will be possible.

Acknowledgements

We acknowledge financial support from DFG through Vo899/6 and Vo899/11 as well as computing resources from ZIH at TU Dresden. Further we would like to thank one of the reviewers for the comment on reformulating the terms involving K in the flow equation.

Appendix. A primer in differential geometry

We derive the viscous stress terms for fluid flow on manifolds in § A.5, in which we follow Arroyo & DeSimone (2009). The stream function formulation is obtained in § A.6. The required fundamentals of exterior differential calculus necessary to accomplish this are provided in § A.2 on exterior calculus, § A.3 on intrinsic formulation of differential operators and finally § A.4 on Laplacians for vector fields. Basic terms are defined in § A.1. For a more comprehensive presentation, see Fraenkel (1997).

A.1. *Basic notation*

Although we aim at an intrinsic description of fluid motion independent of the embedding of the two-dimensional manifold in three-dimensional Euclidean space, it is helpful to have the Euclidean coordinates X of the points of the manifold in Euclidean space available. For the intrinsic description we use local coordinates x^1, x^2. The corresponding basis vectors of the tangential space TM_x at $\boldsymbol{x}$ are $e_i = (\partial X/\partial x^i)$ – but the embedding in $\mathbb{R}^3$ is not necessary to define the tangential vectors. In an intrinsic description we define $\boldsymbol{e}_i$ to be the vector corresponding to the directional derivative $(\partial f/\partial x^i)$ of a function f on the manifold. The tangential space is in this setting the vector space of directional derivatives of C^∞-functions. The dual space of the tangential space is the cotangential space – the space of linear forms on TM_x, where the canonical basis is given by dx^i with $dx^i(\boldsymbol{e}_j) = \delta_{ij}$.

Upper and lower indices are used to indicate the transformation properties of objects. A covariant object is indicated by a lower index, a contravariant object is indicated by an upper index. When a coordinate transformation $\tilde{x} = F(x)$ is applied, a contravariant object v^j transforms via $\tilde{v}^j = (\partial \tilde{x}^j/\partial x^i)v^i$, whereas a covariant object transforms via $\tilde{v}_j = (\partial x^i/\partial \tilde{x}^j)v_i$. This is valid for tensors of higher level, too. The Einstein summation convention is applied throughout this section – summation over pairs of equal upper/lower indices is implicitly assumed.

Our manifold is a Riemannian manifold if it is equipped with a Riemannian metric $\langle v^i \boldsymbol{e}_i, v^j \boldsymbol{e}_j \rangle = v^i v^j g_{ij}$, where g_{ij} is the metric tensor. When an embedding is present, the metric tensor is defined by the Euclidean inner product of tangent vectors $g_{ij} = \langle e_i, e_j \rangle$. The adjoint basis e^i of the tangential space is defined by $\langle e^i, e_j \rangle = \delta_{ij}$. The inverse metric tensor is denoted by $g^{ij} = \langle e^i, e^j \rangle$. A vector $\boldsymbol{v} \in TM_x$ is defined in terms of contravariant coordinates $v = v^i e_i$ or covariant coordinates with respect to the adjoint base $v = v_i e^i$, where raising and lowering of indices is accomplished by the metric tensors $v^i = g^{ij} v_j$ and $v_i = g_{ij} v^j$.

Finally $\sqrt{g} := \sqrt{\det g_{ij}}$ is the stretch of area in local coordinates to area on the manifold, i.e. $\mathrm{d}A = \sqrt{g}\mathrm{d}x^1\mathrm{d}x^2$.

The differentiation of vector fields $\boldsymbol{v}$ along tangent vectors $\boldsymbol{w}$ requires additional concepts because tangent spaces at different points have to be mapped onto. When an embedding is present this is done by a parallel translation and a projection. In a purely intrinsic formulation this is accomplished by the Levi-Civita connection $\boldsymbol{\nabla}_{\boldsymbol{w}} \boldsymbol{v}$. Using the Christoffel symbols Γ^k_{ij} it is expressed in local coordinates

$$\boldsymbol{\nabla}_{\boldsymbol{e}_i} \boldsymbol{e}_j = \Gamma^k_{ij} \boldsymbol{e}_k, \tag{A 1}$$

$$\boldsymbol{\nabla}_{w^i \boldsymbol{e}_i} v^j \boldsymbol{e}_j = w^i (\partial_i v^j) \boldsymbol{e}_j + \Gamma^k_{ij} w^i v^j \boldsymbol{e}_k. \tag{A 2}$$

We abbreviate the covariant derivative $\boldsymbol{\nabla}_i := \boldsymbol{\nabla}_{\boldsymbol{e}_i}$ and the derivative of scalar functions $\partial_i = (\partial / \partial x^i)$.

A.2. *Exterior differential calculus*

The generalization of differential operators like div, grad, rot to Riemannian manifolds can be accomplished in an elegant way by identifying the tangent space and the cotangent space (space of linear forms) of the manifold.

The connection between linear forms $a = a_i \mathrm{d}x^i \in T^* M_x$ at $x \in M$ and tangent vectors $\boldsymbol{v} \in TM_x$ is established by the metric

$$\langle \boldsymbol{v}, \boldsymbol{w} \rangle = a(\boldsymbol{w}), \quad \forall\ \boldsymbol{w} \in TM_x. \tag{A 3}$$

We simply identify the vectors $\boldsymbol{e}^i$ of the adjoint basis of the tangent space with the basis forms $\mathrm{d}x^i$ of the dual space. Moreover, we can identify 2-forms with 2-vectors via

$$\alpha_{12} \mathrm{d}x^1 \wedge \mathrm{d}x^2 = \alpha_{12} \boldsymbol{e}^1 \wedge \boldsymbol{e}^2 = \alpha^{12} \boldsymbol{e}_1 \wedge \boldsymbol{e}_2, \tag{A 4}$$

$$\alpha^{12} = g^{1i} g^{2j} \alpha_{ij} = \frac{1}{g} \alpha_{12}. \tag{A 5}$$

By identifying vectors with forms, we are able to apply exterior differential calculus.

At the heart of exterior differential calculus are k-forms and the exterior differential d, which maps k-forms to $(k+1)$-forms. Functions on the manifold are 0-forms, whereas the general k-form is an alternating k-linear form. The space of k-forms is denoted by Λ^k. A basis of the space of k-forms is formed by

$$\mathrm{d}x^{i_1} \wedge \cdots \wedge \mathrm{d}x^{i_k}, \quad i_1 < \cdots < i_k, \tag{A 6}$$

where

$$\mathrm{d}x^{i_1} \wedge \cdots \wedge \mathrm{d}x^{i_k}(\boldsymbol{e}_{j_1}, \ldots, \boldsymbol{e}_{j_k}) := \begin{cases} 1 & \text{if } (j_1, \ldots, j_k) \text{ is an even permutation of } (i_1, \ldots, i_k), \\ -1 & \text{if } (j_1, \ldots, j_k) \text{ is an odd permutation of } (i_1, \ldots, i_k), \\ 0 & \text{otherwise.} \end{cases} \tag{A 7}$$

For a two-dimensional manifold we have the two-dimensional space of 1-forms Λ^1 with basis forms $\mathrm{d}x^1, \mathrm{d}x^2$, and the one-dimensional space of 2-forms Λ^2 with basis form $\mathrm{d}x^1 \wedge \mathrm{d}x^2$, where

$$\mathrm{d}x^1 \wedge \mathrm{d}x^2(\boldsymbol{v}, \boldsymbol{w}) = v^1 w^2 - v^2 w^1. \tag{A 8}$$

The exterior differential is uniquely defined by the linearity, by $\mathrm{d}f$ being the usual differential for functions $f \in \Lambda^0$, by $\mathrm{dd} = 0$ and the anti-derivative property $\mathrm{d}(\alpha \wedge \beta) = \mathrm{d}\alpha \wedge \beta + (-1)^p \alpha \wedge \mathrm{d}\beta$ whenever α is a p-form. On a two-dimensional closed manifold we have the de Rham complex

$$0 \;\rightarrow\; \Lambda^0 \rightarrow^d \Lambda^1 \rightarrow^d \Lambda^2 \rightarrow^d 0. \tag{A 9}$$

A form α is said to be closed when $\mathrm{d}\alpha = 0$. It is said to be exact when $\alpha = \mathrm{d}\beta$. The property $\mathrm{dd} = 0$ states that every exact form is closed. When every closed form is exact, the complex is said to be exact. For a closed two-dimensional manifold topologically equivalent to the 2-sphere we have that every closed 1-form is exact.

The Hodge star operator $*$ maps a k-form to a $(2-k)$-form on a two-dimensional manifold. For tangent vectors, the Hodge star operator is the (up to sign) unique isometric section of the tangent bundle with the property $\langle *\boldsymbol{v}, \boldsymbol{v}\rangle = 0$.

Finally, the codifferential δ is the adjoint operator of the differential, i.e. $\delta = \mathrm{d}*$. The adjoint property is defined with respect to the metric induced on forms by the Riemannian metric. For a two-dimensional manifold we have $\delta = - * \mathrm{d} *$.

In the setting above we obtain local coordinate expressions for the Hodge star operator $* : \Lambda^i \rightarrow \Lambda^{2-i}$,

$$*f = \sqrt{g} f \mathrm{d}x^1 \wedge \mathrm{d}x^2, \quad f \in \Lambda^0, \tag{A 10}$$

$$*(v^i \boldsymbol{e}_i) = \sqrt{g}(v^1 \boldsymbol{e}^2 - v^2 \boldsymbol{e}^1) = \frac{1}{\sqrt{g}}(v_1 \boldsymbol{e}_2 - v_2 \boldsymbol{e}_1), \tag{A 11}$$

$$*(\alpha_{12} \mathrm{d}x^1 \wedge \mathrm{d}x^2) = \frac{1}{\sqrt{g}} \alpha_{12}, \tag{A 12}$$

the exterior derivative, $\mathrm{d} : \Lambda^i \rightarrow \Lambda^{i+1}$

$$\mathrm{d}f = \frac{\partial f}{\partial x^i} \mathrm{d}x^i = \frac{\partial f}{\partial x^i} \boldsymbol{e}^i = \boldsymbol{\nabla} f, \tag{A 13}$$

$$\mathrm{d}\boldsymbol{v} = \left(\frac{\partial v_2}{\partial x^1} - \frac{\partial v_1}{\partial x^2} \right) \mathrm{d}x^1 \wedge \mathrm{d}x^2, \tag{A 14}$$

and the codifferential $\delta : \Lambda^{i+1} \rightarrow \Lambda^i$, $\delta = - * d *$,

$$\delta \boldsymbol{v} = -\frac{1}{\sqrt{g}} \frac{\partial}{\partial x^i} \sqrt{g} v^i = -\boldsymbol{\nabla} \cdot \boldsymbol{v}, \tag{A 15}$$

$$\delta(\alpha^{12} \boldsymbol{e}_1 \wedge \boldsymbol{e}_2) = \frac{1}{\sqrt{g}} \left(\frac{\partial}{\partial x^2}(\sqrt{g}\alpha^{12}) e_1 - \frac{\partial}{\partial x^1}(\sqrt{g}\alpha^{12}) e_2 \right). \tag{A 16}$$

A.3. *Intrinsic description of differential operators*

By identifying tangent vectors with 1-forms the first-order differential operators grad and div and the second-order Laplace–Beltrami operator Δ_Γ are given in terms of exterior calculus by

$$\mathrm{grad} f = \mathrm{d}f, \tag{A 17}$$

$$\operatorname{div} \boldsymbol{v} = -\delta \boldsymbol{v}, \tag{A 18}$$

$$\Delta_\Gamma f = \operatorname{div} \operatorname{grad} f = -\delta \mathrm{d} f. \tag{A 19}$$

By utilizing the Hodge star operator $*$ we define curl-like operators on a manifold via

$$\operatorname{rot} : \Lambda^1 \to \Lambda^0, \qquad \operatorname{rot} v := *\mathrm{d}\boldsymbol{v} = \delta * \boldsymbol{v}, \tag{A 20}$$

$$\operatorname{Rot} : \Lambda^0 \to \Lambda^1, \qquad \operatorname{Rot} f := *\mathrm{d} f = -\delta * f. \tag{A 21}$$

For the first-order differential operators $\operatorname{div}, \operatorname{grad}, \operatorname{rot}, \operatorname{Rot}$ and the second-order Laplace–Beltrami operator Δ_Γ we have the relations

$$\operatorname{rot} \operatorname{Rot} = *\mathrm{d} * \mathrm{d} = -\delta \mathrm{d} = \Delta_\Gamma, \tag{A 22}$$

$$\operatorname{rot} \operatorname{grad} = 0, \tag{A 23}$$

$$\operatorname{div} \operatorname{Rot} = 0. \tag{A 24}$$

Because every closed 1-form is exact, $\mathrm{d}\boldsymbol{v} = 0$ implies $\boldsymbol{v} = \mathrm{d} f$, or, equivalently, $\delta \boldsymbol{v} = 0$ implies $\boldsymbol{v} = *\mathrm{d} f$; we conclude that Rot maps *onto* the space of divergence-free vector fields. This property justifies the stream function approach.

A.4. *The Laplacian for vector fields*

The generalization of the Laplacian for vector fields from Euclidean space to manifolds is not unique.

We mention here the Hodge–de Rham Laplacian (derived from the vector identity $\Delta \boldsymbol{v} = \operatorname{grad} \operatorname{div} \boldsymbol{v} - \boldsymbol{\nabla} \times (\boldsymbol{\nabla} \times \boldsymbol{v})$) given in terms of exterior calculus by

$$\Delta_\Gamma^R \boldsymbol{v} = -(\mathrm{d}\delta + \delta \mathrm{d})\boldsymbol{v}. \tag{A 25}$$

For incompressible flow we have $\delta \boldsymbol{v} = 0$ and thus $\Delta_\Gamma^R = -\delta \mathrm{d}$.

The Bochner Laplacian (or rough Laplacian) is defined via

$$\Delta_\Gamma^B \boldsymbol{v} := -\boldsymbol{\nabla}^* \boldsymbol{\nabla} \boldsymbol{v}, \tag{A 26}$$

where the gradient operator has to be generalized to forms. In local coordinates we obtain

$$\Delta_\Gamma^B \boldsymbol{v} = \frac{1}{\sqrt{g}} \boldsymbol{\nabla}_j \sqrt{g} \boldsymbol{\nabla}_{\boldsymbol{e}^j} \boldsymbol{v}. \tag{A 27}$$

The two operators are related by the Weitzenböck identity

$$\Delta_\Gamma^B \boldsymbol{v} = \Delta_\Gamma^R \boldsymbol{v} + K \boldsymbol{v} \tag{A 28}$$

where K is Gaussian curvature.

For a more detailed treatise of Laplacians, see Arroyo & DeSimone (2009).

A.5. *Derivation of viscous terms in the Navier–Stokes equations on a manifold*

The relative rate of change of the length of tangential vectors $\boldsymbol{x}$ under a flow field $\boldsymbol{v}$ on a manifold is given by $\langle \boldsymbol{\nabla}_{\boldsymbol{x}} \boldsymbol{v}, \boldsymbol{x} \rangle$, which defines the symmetric strain rate tensor

$$\varepsilon(\boldsymbol{x}, \boldsymbol{y}) := \tfrac{1}{2}(\langle \boldsymbol{\nabla}_{\boldsymbol{x}} \boldsymbol{v}, \boldsymbol{y} \rangle + \langle \boldsymbol{\nabla}_{\boldsymbol{y}} \boldsymbol{v}, \boldsymbol{x} \rangle). \tag{A 29}$$

The contravariant representation $\varepsilon = \varepsilon^{ij} \boldsymbol{e}_i \otimes \boldsymbol{e}_j$ is given in local coordinates by

$$\varepsilon^{ij} = \varepsilon(\boldsymbol{e}^i, \boldsymbol{e}^j) = \tfrac{1}{2}(\langle \boldsymbol{\nabla}_{\boldsymbol{e}^i} \boldsymbol{v}, \boldsymbol{e}^j \rangle + \langle \boldsymbol{\nabla}_{\boldsymbol{e}^j} \boldsymbol{v}, \boldsymbol{e}^i \rangle). \tag{A 30}$$

The resulting forces $\boldsymbol{f}$ on line elements of length $\mathrm{d}s$ with normal $\boldsymbol{n} = n_j \boldsymbol{e}^j$ depend linearly on $\boldsymbol{n}\mathrm{d}s$, where the relation is given by the stress tensor τ: $\boldsymbol{f} = \tau \boldsymbol{n}\mathrm{d}s$, $f^i = \tau^{ij} n_j \mathrm{d}s$. The constitutive law relates the strain rate tensor to the stress tensor. For Newtonian fluids stress τ depends linearly on the strain, $\tau = 2\mu\varepsilon$. For flow on manifolds this relation is assumed for the principal components of the strain rate tensor. This is accomplished by

$$\langle \tau \boldsymbol{n}, y \rangle = 2\mu\varepsilon(\boldsymbol{n}, \boldsymbol{y}), \quad \forall\, \boldsymbol{y}, \tag{A 31}$$

$$\Rightarrow \quad \langle \tau \boldsymbol{e}^i, \boldsymbol{e}^j \rangle = 2\mu\varepsilon(\boldsymbol{e}^i, \boldsymbol{e}^j), \tag{A 32}$$

$$\text{i.e.} \qquad \tau^{ij} = 2\mu\varepsilon^{ij} = \mu(\langle \nabla_{e^i} v, e^j \rangle + \langle \nabla_{e^j} v, e^i \rangle). \tag{A 33}$$

The resulting force acting on fluid particles in an area Ω with boundary Γ is obtained by a boundary integral, where we have to interpret the forces for a moment as vectors in $\mathbb{R}^3$. Nevertheless, if we utilize the Levi-Civita connection in the divergence operator, the application of the Gauss theorem gives just the components tangential to the manifold

$$\int_\Gamma n_i \tau^{ij} e_j \,\mathrm{d}s = \int_\Omega \frac{1}{\sqrt{g}} \nabla_i (\sqrt{g} \tau_{ij} e_j) \,\mathrm{d}x. \tag{A 34}$$

We end up with the force term

$$\boldsymbol{F}_{visc} = \frac{\mu}{\sqrt{g}} \nabla_i \sqrt{g} (\nabla_{\boldsymbol{e}^i} v + \langle \nabla_{\boldsymbol{e}^j} \boldsymbol{v}, \boldsymbol{e}^i \rangle \boldsymbol{e}_j). \tag{A 35}$$

We show below that this simplifies to $\mu(\Delta_\Gamma^B \boldsymbol{v} + K\boldsymbol{v})$. The first term is easily identified as $\mu \Delta_\Gamma^B \boldsymbol{v}$. The second term in the viscous force evaluates to the curvature term

$$\frac{1}{\sqrt{g}} \nabla_i \sqrt{g} \langle \nabla_{\boldsymbol{e}^j} \boldsymbol{v}, \boldsymbol{e}^i \rangle \boldsymbol{e}_j \tag{A 36}$$

$$= \frac{1}{\sqrt{g}} \nabla_i \sqrt{g} \langle \nabla_j, \boldsymbol{e}^i \rangle \boldsymbol{e}^j \tag{A 37}$$

$$= \frac{1}{\sqrt{g}} \nabla_i \langle \nabla_j \sqrt{g} \boldsymbol{v}, \boldsymbol{e}^i \rangle \boldsymbol{e}^j - \frac{1}{\sqrt{g}} \nabla_i \sqrt{g} v^i \frac{1}{\sqrt{g}} (\partial_j \sqrt{g}) e^j \tag{A 38}$$

$$= \frac{1}{\sqrt{g}} \nabla_i \left((\partial_j \sqrt{g} \boldsymbol{v}^i) \boldsymbol{e}^j + \sqrt{g} v^k \langle \nabla_j \boldsymbol{e}_k, \boldsymbol{e}^i \rangle \boldsymbol{e}^j \right) - v^i \nabla_i \frac{1}{\sqrt{g}} (\partial_j \sqrt{g}) e^j \tag{A 39}$$

$$= \frac{1}{\sqrt{g}} (\partial_j \sqrt{g} \boldsymbol{v}^i) \nabla_i \boldsymbol{e}^j - \frac{1}{\sqrt{g}} \nabla_i \left(\sqrt{g} v \nabla_k \boldsymbol{e}^i \right) - v^i \nabla_i \frac{1}{\sqrt{g}} (\partial_j \sqrt{g}) \boldsymbol{e}^j \tag{A 40}$$

$$= -v^k \nabla_i \nabla_k \boldsymbol{e}^i - v^k \nabla_k (\Gamma_{ij}^i \boldsymbol{e}^j) = v^k (\nabla_k \nabla_i - \nabla_i \nabla_k) \boldsymbol{e}^i \tag{A 41}$$

$$= v^1 (\nabla_1 \nabla_2 - \nabla_2 \nabla_1) \boldsymbol{e}^2 + v^2 (\nabla_2 \nabla_1 - \nabla_1 \nabla_2) \boldsymbol{e}^1 = Kv. \tag{A 42}$$

For the final step, see Fraenkel (1997, § 8.5).

A.6. *Intrinsic description with a stream function*

The advection operator is given in intrinsic terms by the Levi-Civita connection $\nabla_{\boldsymbol{v}}$ on the Riemannian manifold

$$\frac{\mathrm{D}}{\mathrm{D}t} \boldsymbol{v} = \frac{\partial \boldsymbol{v}}{\partial t} + \nabla_{\boldsymbol{v}} \boldsymbol{v}. \tag{A 43}$$

A more convenient form is given by the vector identity

$$\nabla_{\boldsymbol{v}}\boldsymbol{v} = \tfrac{1}{2}\nabla\langle\boldsymbol{v},\boldsymbol{v}\rangle + (*\boldsymbol{v})\,\mathrm{rot}\,\boldsymbol{v}, \tag{A 44}$$

which is derived easily in our setting as

$$\begin{aligned}\nabla_{\boldsymbol{v}}\boldsymbol{v} - 1/2\nabla\langle\boldsymbol{v},\boldsymbol{v}\rangle &= v^i\nabla_i\boldsymbol{v} - \frac{1}{2}(\partial_j\langle\boldsymbol{v},\boldsymbol{v}\rangle)e^j\\ &= v^i\langle\nabla_i\boldsymbol{v},\boldsymbol{e}_j\rangle\boldsymbol{e}^j - \langle\nabla_j\boldsymbol{v},\boldsymbol{v}\rangle e^j = v^i\boldsymbol{e}^j(\langle\nabla_i\boldsymbol{v},\boldsymbol{e}_j\rangle - \langle\nabla_j\boldsymbol{v},\boldsymbol{e}_i\rangle)\\ &= \sqrt{g}(v^1\boldsymbol{e}^2 - v^2\boldsymbol{e}^1)\frac{1}{\sqrt{g}}(\langle\nabla_1\boldsymbol{v},\boldsymbol{e}_2\rangle - \langle\nabla_2\boldsymbol{v},\boldsymbol{e}_1\rangle)\\ &= (*\boldsymbol{v})(*\mathrm{d}\boldsymbol{v}).\end{aligned} \tag{A 45}$$

In order to eliminate the zero-divergence condition (2.17) we substitute

$$v = \mathrm{Rot}\,\psi = *\mathrm{d}\psi \tag{A 46}$$

into (2.26) and apply the operator $\mathrm{rot} = *\mathrm{d} = \delta*$. This eliminates all gradient terms (A 23), in particular the gradients of pressure p and kinetic energy. The terms in the Navier–Stokes equations evaluate to

$$\mathrm{rot}\,\boldsymbol{v}_t = \mathrm{rot}\,\mathrm{Rot}\,\psi_t = \Delta_\Gamma\psi_t, \tag{A 47}$$

$$\mathrm{rot}\,\boldsymbol{v} = \Delta_\Gamma\psi, \tag{A 48}$$

and further

$$\nabla_{\boldsymbol{v}}\boldsymbol{v} = (-\mathrm{d}\psi)(\Delta_\Gamma\psi) + \tfrac{1}{2}\mathrm{d}\langle\boldsymbol{v},\boldsymbol{v}\rangle, \tag{A 49}$$

$$\mathrm{rot}\,\nabla_{\boldsymbol{v}}\boldsymbol{v} = -\delta(*\mathrm{d}\psi)(\Delta_\Gamma\psi) = \langle *\mathrm{d}\psi, \mathrm{d}\Delta_\Gamma\psi\rangle, \tag{A 50}$$

$$=: J(\psi, \Delta_\Gamma\psi), \tag{A 51}$$

where $J(f,h) := \langle *\mathrm{d}f, \mathrm{d}h\rangle$ is the so-called Jacobian. In Cartesian coordinates the Jacobian evaluates to $J = f_x h_y - f_y h_x$. Finally,

$$\mathrm{rot}\,\Delta^R_\Gamma\boldsymbol{v} = (\delta*)(-\delta\mathrm{d})(*\mathrm{d}\psi) = (\delta*)(*\mathrm{d}*\mathrm{d})(*\mathrm{d}\psi) \tag{A 52}$$

$$= \delta(-1)\mathrm{d}(*\mathrm{d}*)\mathrm{d}\psi = \delta\mathrm{d}\delta\mathrm{d}\Psi \tag{A 53}$$

$$= \Delta_\Gamma\Delta_\Gamma\Psi \tag{A 54}$$

$$\mathrm{rot}\,K\boldsymbol{v} = K\Delta_\Gamma\psi + \langle\nabla_\Gamma\psi, \nabla_\Gamma K\rangle = \nabla_\Gamma\cdot(K\nabla_\Gamma\psi). \tag{A 55}$$

We end up with a scalar partial differential equation for the stream function ψ on a manifold

$$\partial_t\Delta_\Gamma\psi + J(\psi, \Delta_\Gamma\psi) = \mu(\Delta^2_\Gamma\psi + 2\nabla_\Gamma\cdot(K\nabla_\Gamma\psi)) + f, \tag{A 56}$$

where $f = \mathrm{rot}\,F$. For computational purposes it is convenient to represent tangent vectors of a two-dimensional manifold as vectors in three-dimensional Euclidean space. In this setting the Hodge star operator translates to a rotation of 90° in the tangential plane and the metric is replaced by the Euclidean scalar product.

REFERENCES

ALAND, S. & VOIGT, A. 2012 Benchmark computations of diffuse interface models for two-dimensional bubble dynamics. *Intl J. Numer. Meth. Fluids* **69**, 747–761.

ARROYO, M. & DESIMONE, A. 2009 Relaxation dynamics of fluid membranes. *Phys. Rev.* E **79**, 031915.

BERTALMIO, M., CHENG, L. T., OSHER, S. & SAPIRO, G. 2001 Variational problems and partial differential equations on implicit surfaces. *J. Comput. Phys.* **174**, 759–780.

BONITO, A., NOCHETTO, R. & PAULETTI, M. S. 2010 Parametric FEM for geometric biomembranes. *J. Comput. Phys.* **229**, 3171–3188.

BOTHE, D. & PRUESS, J. 2010 On the two-phase Navier–Stokes equations with Boussinesq–Scriven surface fluid. *J. Math. Fluid Mech.* **12**, 133–150.

BOWICK, M. J. & GIOMI, L. 2009 Two-dimensional matter: order, curvature and defects. *Adv. Phys.* **58**, 449–563.

CAO, C. S., RAMMAHA, M. A. & TITI, E. S. 1999 The Navier–Stokes equations on a rotating 2-d sphere: Gevrey regularity and asymptotic degrees of freedom. *Z. Angew. Math. Phys.* **50**, 341–360.

DZIUK, G. 1991 An algorithm for evolutionary surfaces. *Numer. Math.* **58**, 603–611.

DZIUK, G. & ELLIOTT, C. M. 2007*a* Finite elements on evolving surfaces. *IMA J. Numer. Anal.* **27**, 262–292.

DZIUK, G. & ELLIOTT, C. M. 2007*b* Surface finite elements for parabolic equations. *J. Comput. Math.* **25**, 385–407.

EBIN, D. G. & MARSDEN, J. 1970 Groups of diffeomorphisms and motion of an incompressible fluid. *Ann. Maths* **92**, 102.

ELLIOTT, C. M. & STINNER, B. 2009 Analysis of a diffuse interface approach to an advection diffusion equation on a moving surface. *Math. Models Meth. Appl. Sci.* **19**, 787–802.

ELLIOTT, C. M. & STINNER, B. 2011 A surface phase field model for two-phase biological membranes. *SIAM J. Appl. Math.* **70**, 2904–2928.

FAN, J., HAN, T. & HAATAJA, M. 2010 Hydrodynamic effects on spinodal decomposition kinetics in planar lipid bilayer membranes. *J. Chem. Phys.* **133**, 235101.

FENG, X. 2006 Fully discrete finite element approximations of the Navier–Stokes–Cahn–Hilliard diffuse interface model for two-phase fluid flows. *SIAM J. Numer. Anal.* **44**, 1853–1866.

FRAENKEL, T. 1997 *The Geometry of Physics: An Introduction*. Cambridge University Press.

GOMEZ, H. & HUGHES, T. J. R. 2011 Provable unconditionally stable, second-order time-accurate, mixed variational methods for phase-field models. *J. Comput. Phys.* **230**, 5310–5327.

HEINE, C.-J. 2004 Isoparametric finite element approximation of curvature on hypersurfaces. Preprint, No. 26, Fakultät für Mathematik und Physik, Universität Freiburg.

HOHENBERG, P. C. & HALPERIN, B. I. 1977 Theory of dynamic critical phenomena. *Rev. Mod. Phys.* **49**, 435–479.

HU, D., ZHANG, P. W. & E, W. 2007 Continuum theory of moving membrane. *Phys. Rev.* E **75**, 041605.

KWON, Y., THORNTON, K. & VOORHEES, P. W. 2010 Morphology and topology in coarsening of domains via non-conserved and conserved dynamics. *Phil. Mag.* **90**, 317–335.

LARADJI, M. & KUMAR, P. B. 2006 Anomalously slow domain growth in fluid membranes with asymmetric transbilayer lipid distribution. *Phys. Rev.* E **73**, 040901.

LI, S., LOWENGRUB, J., RÄTZ, A. & VOIGT, A. 2009 Solving PDEs in complex geometries: a diffuse domain approach. *Commun. Math. Sci.* **7**, 81–107.

LOWENGRUB, J. S., RÄTZ, A. & VOIGT, A. 2009 Phase-field modelling of the dynamics of multicomponent vesicles: spinodal decomposition, coarsening, budding, and fission. *Phys. Rev.* E **79**, 031926.

LOWENGRUB, J. & TRUSKINOWSKY, L. 1998 Quasi-incompressible Cahn–Hilliard fluids and topological transitions. *Proc. R. Soc. Lond.* A **454**, 2617–2654.

MACDONALD, C. B. & RUUTH, S. J. 2009 The implicit closest point method for the numerical solution of partial differential equations on surfaces. *SIAM J. Sci. Comput.* **31**, 4330–4350.

MEYER, M., DESBRUN, M., SCHRÖDER, P. & BARR, A. H. 2003 Discrete differential-geometry operators for triangulated 2-manifolds. In *Visualization and Mathematics III* (ed. H.-C. Hege & K. Ploltier), pp. 59–68. Springer.

MITREA, M. & TAYLOR, M. 2001 Navier–Stokes equations on Lipschitz domains in Riemannian manifolds. *Math. Ann.* **321**, 955–987.

NEAMTAN, S. M. 1946 The motion of harmonic waves in the atmosphere. *J. Meteorol.* **3**, 43–56.

RAMACHANDRAN, S., KOMURA, S. & GOMPPER, G. 2010 Effects of an embedding bulk fluid on phase separation dynamics in a thin liquid film. *Eur. Phys. Lett.* **89**, 56001.

RAMACHANDRAN, S., LARADJI, M. & KUMAR, P. B. 2009 Lateral organisation of lipids in multi-component liposomes. *J. Phys. Soc. Japan* **78**, 041006.

RÄTZ, A. & VOIGT, A. 2006 PDEs on surfaces – a diffuse interface approach. *Commun. Math. Sci.* **4**, 575–590.

RÄTZ, A. & VOIGT, A. 2007 A diffuse-interface approximation for surface diffusion including adatoms. *Nonlinearity* **20**, 177–192.

RUUTH, S. J. & MERRIMAN, B. 2008 A simple embedding method for solving partial differential equations on surfaces. *J. Comput. Phys.* **227**, 1943–1961.

SAEKI, D., HAMADA, T. & YOSHIKAWA, K. 2006 Domain-growth kinetics in a cell-sized liposome. *J. Phys. Soc. Japan* **75**, 013602.

SAFMANN, P. G. & DELBRUECK, M. 1975 Brownian motion in biological membranes. *Proc. Natl Acad. Sci.* **72**, 3111–3113.

SCRIVEN, L. E. 1960 Dynamics of fluid interfaces. Equations of motion for Newtonian surface fluids. *Chem. Engng Sci.* **12**, 98–108.

STÖCKER, C. & VOIGT, A. 2008 Geodesic evolution laws – a level set approach. *SIAM J. Imag. Sci.* **1**, 379–399.

TANIGUCHI, T. 1996 Shape deformation and phase separation dynamics of two-component vesicles. *Phys. Rev. Lett.* **76**, 4444–4447.

TEMAM, R. 1988 *Infinite-Dimensional Dynamical Systems in Mechanics and Physics*. Springer.

TURNER, A. M., VITELLI, V. & NELSON, D. R. 2010 Vortices on curved surfaces. *Rev. Mod. Phys.* **82**, 1301–1348.

VEATCH, S. L. & KELLER, S. L. 2003 Separation of liquid phases in giant vesicles of ternary mixtures of phospholipids and cholesterol. *Biophys. J.* **85**, 3074–3083.

VEY, S. & VOIGT, A. 2007 AMDIS – adaptive multidimensional simulations. *Comput. Vis. Sci.* **10**, 57–66.

WANG, X. Q. & DU, Q. 2008 Modelling and simulations of multi-component lipid membranes and open membranes via diffuse interface approaches. *J. Math. Biol.* **56**, 347–371.

YANAGISAWA, M., IMAL, M., MASUI, T., KOMURA, S. & OHTA, T. 2007 Dynamics of domains in ternary fluid vesicles. *Biophys. J.* **92**, 115–125.

ZIENKIEWICZ, O. C. & ZHU, J. Z. 1987 A simple error estimator and adaptive procedure for practical engineering analysis. *Intl J. Numer. Meth. Engng* **24**, 337–357.